Modeling Spin-Forbidden Monomer Self-Initiation Reactions in Spontaneous Free-Radical Polymerization of Acrylates and Methacrylates

Shi Liu,[†] Sriraj Srinivasan,[‡] Jianmin Tao,[†] Michael C. Grady,[§] Masoud Soroush,[∥] and Andrew M. Rappe*,[†]

[†]The Makineni Theoretical Laboratories, Department of Chemistry, University of Pennsylvania, Philadelphia, Pennsylvania 19104-6323, United States

[‡]Arkema Inc., 900 First Avenue, King of Prussia, Pennsylvania 19406, United States

[§]DuPont Experimental Station, Wilmington, Delaware 19898, United States

[∥]Department of Chemical and Biological Engineering, Drexel University, Philadelphia, Pennsylvania 19104, United States

Ⓢ *Supporting Information*

ABSTRACT: A spin-forbidden reaction is a reaction in which the total electronic spin-state changes. The standard transition-state theory that assumes a reaction occurs on a single potential energy surface with spin-conservation cannot be applied to a spin-forbidden reaction directly. In this work, we derive the crossing coefficient based on the Wentzel−Kramers−Brillouin (WKB) theory to quantify the effect of intersystem crossing on the kinetics of spin-forbidden reactions. Acrylates and methacrylates, by themselves, can generate free radicals that initiate polymerization at temperatures above 120 °C. Previous studies suggest that a triplet diradical is a key intermediate in the self-initiation. The formation of a triplet diradical from two closed-shell monomer molecules is a spin-forbidden reaction. This study provides a quantitative analysis of singlet−triplet spin crossover of diradical species in self-initiation of acrylates and methacrylates, taking into account the effect of intersystem crossing. The concept of crossing control is introduced and demonstrated computationally to be a new likely route to generate monoradicals via monomer self-initiation in high temperature polymerization.
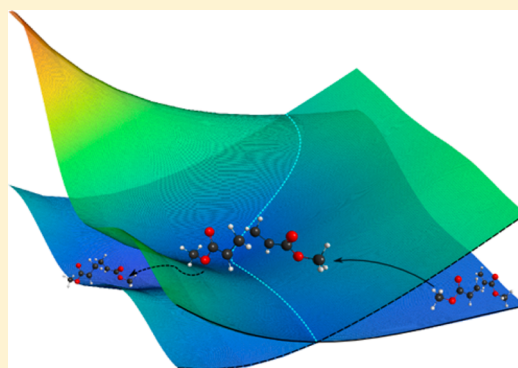
1. INTRODUCTION

The standard transition-state theory has played a paradigmatic role in understanding chemical reactions quantitatively.[1] Based on the Born−Oppenheimer approximation, standard transition-state theory assumes that a transformation proceeds on a single potential energy surface (PES). However, many chemical transformations occur with a change of spin-state involving more than one PES.[2−4] These reactions are "spin-forbidden" because they are formally forbidden in nonrelativistic quantum mechanics. Intersystem crossing refers to the nonradiative transition between two electronic states of different multiplicity.[2] The spin−orbit coupling (SOC), the coupling between the spin angular momentum and its orbital angular momentum, originates from the interactions between the magnetic dipole moment of the electron and the magnetic field associated with the orbital motion of the electron in the electrostatic field of a nucleus,[5] and it gives the mechanism for hopping from one PES to another.[6] Spin-forbidden reactions are common for organometallic reactions because of the degeneracy (or near degeneracy) of d orbitals of the transition metal giving rise to close-lying states with different spin-states.[7,8]

Previous theoretical and experimental studies[9−13] on the spontaneous free-radical polymerization of acrylates revealed

that acrylate monomers can self-initiate at high temperatures, opening a new route for designing initiator-free polymerization processes. It was proposed (Figure 1) that two acrylate (methacrylate) monomers dimerize in a [2 + 2] nonconcerted cycloaddition reaction to form a singlet diradical. The singlet diradical passes to a triplet state nonradiatively, producing a triplet diradical that is energetically more stable. A third acrylate (methacrylate) monomer then abstracts a hydrogen atom from the triplet diradical and two monoradicals are formed.[12] A methacrylate singlet diradical can also transfer a hydrogen atom to a third monomer to form two monoradicals.[9−12] However, a quantitative description of the singlet−triplet crossover, which influences the rate of self-initiation, is not yet available. Previous quantum chemistry calculations showed that the energy barrier of the [2 + 2] cycloaddition reaction of acrylates estimated by B3LYP is about 45 kJ/mol higher than that obtained with MP2 using various basis sets.[10] Such a large discrepancy of the energy barriers predicted by density functional theory (DFT) and a many-body wavefunction-based method is an indication
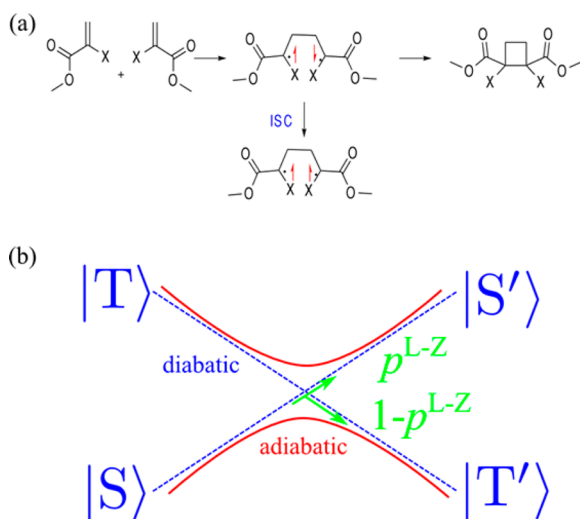
Figure 1. (a) Monomer self-initiation reactions of acrylates and methacrylates (X = H or CH$_3$). (b) Representation of singlet−triplet intersystem crossing.

of the complicated electronic structure of the diradical intermediates[14,15] involved in the monomer self-initiation reactions. In this study, we carried out a benchmark study to evaluate the performance of various density functionals on self-initiation reactions. In addition, the production of a triplet diradical from two singlet monomers is a spin-forbidden reaction requiring the change of spin-state.[4,8,16,17] Standard transition-state theory that assumes the reaction occurs on a single PES with spin-conservation, however, cannot be directly applied to spin-forbidden reactions. This article aims to provide a quantitative description of the monomer self-initiation reaction within the framework of nonadiabatic transition-state theory (NA-TST)[3,18] with full consideration of the effect of intersystem crossing.

The rest of the paper is organized as follows. The derivation of intersystem crossing coefficient within the framework of nonadiabatic transition-state theory is described in Section 2. Section 3 presents the results and discussions. Finally, conclusions are made in Section 4.

2. THEORY AND COMPUTATIONAL METHODS

2.1. Crossing Coefficient in Nonadiabatic Transition-State Theory. In a spin-forbidden reaction involving N atoms, the crossing points between two PESs of different multiplicity form a hypersurface with $3N - 7$ dimensions. The minimum energy crossing point (MECP) is the point with the lowest energy at the crossing hypersurface. The rate coefficient at a given temperature, $k(T)$, is computed based on statistical rate theory[18] using the following equation:

$$k(T) = \frac{1}{hQ_R(T)} \int_0^\infty G_{MECP}(E) e^{-E/k_B T} \, dE \quad (1)$$

where h is Planck's constant, k_B is Boltzmann's constant, $Q_R(T)$ is the partition function of the reactants, and $G_{MECP}(E)$ is the crossing-probability-weighted density of states at the MECP for a given E relative to the zero-point of the reactants. $G_{MECP}(E)$ can be estimated with

$$G_{MECP}(E) = \int_0^E P_c(\varepsilon_h) N_{MECP}(E - \varepsilon_h) \, d\varepsilon_h \quad (2)$$

where $P_c(\varepsilon_h)$ is the crossing probability with energy ε_h along the direction of hopping, and $N_{MECP}(E - \varepsilon_h)$ is the density of states at the MECP with the remaining energy $E - \varepsilon_h$. Therefore, $G_{MECP}(E)$ is simply a semiclassical representation of the number of ways to distribute total energy E between the hopping degree of freedom and the rest of the rotational and vibrational degrees of freedom weighted by the hopping probability. The crossing probability $P_c(\varepsilon_h)$ can be calculated using either the double-passage Landau−Zener (L-Z) formula[19−21] or the Wentzel−Kramers−Brillouin (WKB) theory.[18,22,23] The double-passage L-Z formula for the crossing probability is given by

$$P_c^{L-Z}(\varepsilon_h) = 2\left[1 - \exp\left(-\frac{\pi\beta}{4\sqrt{\varepsilon}}\right)\right] \quad (3)$$

while the WKB theory gives the crossing probability as

$$P_c^{WKB}(\varepsilon_h) = \pi^2 \beta^{4/3} \mathrm{Ai}^2(-\varepsilon\beta^{2/3}) \quad (4)$$

where

$$\beta = \frac{4H_{12}^{3/2}}{\hbar}\left(\frac{\mu}{F\Delta F}\right)^{1/2} \qquad \varepsilon = (\varepsilon_h - E_c)\varepsilon_0$$

$$\varepsilon_0 = \frac{\Delta F}{2FH_{12}}$$

$$\Delta F = |F_1 - F_2| \qquad F = |F_1 F_2|^2$$

Ai is the Airy function, E_c is the crossing energy, μ is the reduced mass orthogonal to the seam of crossing, and F_1 and F_2 are the gradients of PESs with different multiplicity at the MECP. H_{12} is the spin−orbit coupling matrix element $\langle \Psi_1 | H_{SO} | \Psi_2 \rangle$, in which H_{so} is the two-electron Breit−Pauli spin−orbit operator.[24−27] The factor of 2 in the L-Z formula in eq 3 takes into account the transition events that occur via both a single passage and a double passage (not crossing on the first passage but crossing during the second passage) through the crossing region:

$$P_c^{L-Z}(\varepsilon_h) = (1 - p^{L-Z}) + p^{L-Z}(1 - p^{L-Z})$$

$$\approx 2(1 - p^{L-Z}) \quad (5)$$

where

$$1 - p^{L-Z} \ll p^{L-Z},$$

$$p^{L-Z} = \exp\left(-\frac{\pi\beta}{4\sqrt{\varepsilon}}\right) = \exp\left(-\frac{2\pi H_{12}^2}{\Delta F \hbar \sqrt{\frac{2(\varepsilon_h - E_c)}{\mu}}}\right)$$

p^{L-Z}, as illustrated in Figure 1b, is the Landau−Zener probability of hopping from one adiabatic state to another adiabatic state (in other words, remaining in the initial diabatic state), and $(1 - p^{L-Z})$ is the hopping probability from one diabatic state to the other diabatic state. However, the L-Z formula fails to account for the crossing at energies below E_c because ε_h must be larger than E_c in order to apply eqs 3 and 5. The WKB theory, on the other hand, considers the crossing below E_c via the use of the Airy function. Since the crossing barrier is high compared to $k_B T$, most crossings occur in this system for $\varepsilon_h < E_c$. Therefore we apply eq 4 based on the WKB theory to quantify the crossing probability.

Using eqs 1 and 2, and the property of the Laplace transform

$$\mathcal{L}\left\{ \int_0^E f_1(x) f_2(E-x)\, dx \right\}$$

$$= \mathcal{L}\{f_1(x)\}\mathcal{L}\{f_2(x)\}$$

$$= F_1(s) F_2(s)$$

we obtain

$$k(T) = \frac{P(T)}{h}\frac{Q_{MECP}(T)}{Q_R(T)} \tag{6}$$

where $P(T)$ is the Laplace transform of $P_c(\varepsilon_h)$ and $Q_{MECP}(T)$ is the partition function of the MECP ($s = 1/k_B T$ is used in the Laplace transform). Based on the WKB theory, we can approximate the rate constant (see detailed derivations in the Supporting Information) with

$$k(T) = \Gamma(T)\frac{k_B T}{h}\frac{Q_{MECP}(T)}{Q_R(T)} e^{-E_c/k_B T} \tag{7}$$

where the crossing coefficient, $\Gamma(T)$, is given by

$$\Gamma(T) = \frac{\pi^{3/2}\beta}{2\sqrt{\varepsilon_0/(k_B T)}}\left[1 + \frac{1}{2}\exp\left(\frac{1}{12\beta^2}\frac{1}{(k_B T\varepsilon_0)^3} \right) \right] \tag{8}$$

Recall the microscopic rate constant derived in the standard transition-state theory with tunneling corrections[18,28]

$$k^{TST}(T) = \kappa(T)\frac{k_B T}{h}\frac{Q_{TS}(T)}{Q_R(T)} e^{-E_0/k_B T} \tag{9}$$

where $\kappa(T)$ is the tunneling coefficient, Q_{TS} is the partition function of the transition state, and E_0 is the energy barrier. We note that eq 7 is analogous to eq 9, and therefore the MECP in a spin-forbidden reaction can be considered as the "transition state": the barrier is given by the crossing energy and the nonclassical effect that comes from intersystem crossing is incorporated in the crossing coefficient.

2.2. Computational Methods. We carried out a benchmark study to determine cost-effective density functionals for the study of monomer self-initiation reactions. Three composite procedures, CBS-QB3,[29,30] G3(MP2)-RAD,[31] and G4(MP2)-6X,[32−34] are used to investigate three different cycloaddition reactions listed in Figure 2. These composite quantum chemistry methods combine high-level theory (coupled cluster) with relatively small basis sets (e.g., CCSD(T)/6-31G* in G4(MP2)-6X) and low-level theory (Hartree−Fock) with complete basis sets (CBS). The composite procedures are performed with Gaussian 09 program
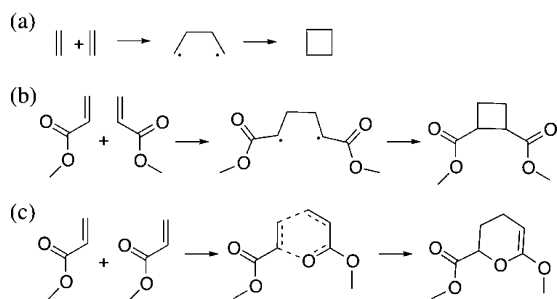
Figure 2. (a) [2 + 2] cycloaddition reaction of ethylene. (b) [2 + 2] cycloaddition reaction of methyl acrylate. (c) [2 + 4] cycloaddition reaction of methyl acrylate.

package.[35] A wide variety of density functionals, B3LYP,[36−38] PBE0,[39] BMK,[40] TPSS,[41] TPSSh,[42] revTPSS,[43] M06-L,[44] M06, M06-2X,[45] and ωB97x-D,[46] and three different basis sets, 6-31G*, 6-311G**, and 6-31+G(2df,p), are used to calculate the same energy barriers. These energy barrier values are then compared with those obtained using the composite procedures. DFT calculations are carried out with GAMESS.[47] Restricted-open-shell Hartree−Fock (ROHF) wavefunctions are used in this study over unrestricted-open-shell Hartree−Fock (UHF) wavefunctions, because previous studies have shown that UHF wavefunctions have the problem of spin contamination for radical reactions.[48,49] Frequency calculations are performed for all the optimized stationary structures (reactants, products, and transition states). The MECPs for various monomer self-initiation reactions are identified with DFT. Spin−orbit coupling constants for these DFT-optimized MECPs are then computed using spin−orbit configuration interaction (SO−CI) method with a multiconfigurational wavefunction of CASSCF (complete active space multiconfiguration self-consistent field) type. The active space of the CASSCF wavefunction is designed to have eight active electrons in eight active orbitals. We also computed the SOC constant using spin−orbit multiconfigurational quasidegenerate second-order perturbation theory (SO-MCQDPT2) with the same active space.[50] Other quantities, such as μ, F_1, and F_2, are calculated by analyzing the vibrational frequencies at the MECP on both singlet and triplet states. The algorithms for the code (GLOWfreq) used for analysis can be found in cited literature.[51,52]

3. RESULTS AND DISCUSSIONS

3.1. Benchmark Study on Cycloaddition Reactions. Tables 1−3 present the energy barriers obtained with the composite procedures and various density functionals with three different basis sets for the [2 + 2] cycloaddition reaction of ethylene, [2 + 2] cycloaddition reaction of MA, and [2 + 4] cycloaddition reaction of MA, respectively. For each of the cycloaddition reactions, we find that the three composite methods predict similar energy barriers. It is seen from Table 1 that for the [2 + 2] cycloaddition reaction of ethylene, CBS-QB3 predicts a barrier of 196 kJ/mol, G3(MP2)-RAD 201 kJ/mol, and G4(MP2)-6X 181 kJ/mol, all agreeing reasonably well with the experimental value of 180 kJ/mol.[53] This indicates that these three composite procedures are reliable for studying cycloaddition reactions. However, many density functionals such as B3LYP, BMK, M06-2X, and ωB97x-D that have been widely used in computational/theoretical study of polymerization reactions significantly overestimate the barrier for [2 + 2] cycloaddition reactions. For the [2 + 2] cycloaddition reactions of MA the results given in Table 2 indicate that the energy barriers predicted by the density functionals, TPSSh, PBE0, TPSS, M06, and M06-L, with the 6-31G* basis set are close to those predicted by the composite method, and the barrier predicted by revTPSS/6-31+G(2df,p) and M06-L/6-31+G(2df,p) are in the best agreement with those predicted by G4(MP2)-6X. As for the [2 + 4] cycloaddition reactions of MA, we observe from Table 3 that the PBE0, TPSS, TPSSh, M06-L, and M06 with the 6-31G* basis set predict barriers with less than 10% absolute percentage deviation. The M06, PBE0, and TPSSh density functionals with a 6-31+G(2df,p) basis set estimate energy barriers with 2% absolute percentage deviation relative to G4(MP2)-6X. However, the computation cost using 6-31+G(2df,p) basis set is significantly higher in comparison to using 6-31G* basis set. This benchmark study also indicates

Table 1. Energy Barrier (E_0) in kJ/mol for [2 + 2] Cycloaddition Reaction of Ethylene and Absolute Percent Deviation (APD) Relative to G4(MP2)-6X for Various Density Functionals and Basis Sets

B3LYP	E_0 (APD)	PBE0	E_0 (APD)	BMK	E_0 (APD)	TPSS	E_0 (APD)	TPSSh	E_0 (APD)
6-31G*	262 (30.4%)	6-31G*	242 (20.6%)	6-31G*	268 (33.8%)	6-31G*	230 (14.5%)	6-31G*	243 (21.3%)
6-311G**	271 (35.2%)	6-311G**	248 (23.6%)	6-311G**	277 (38.1%)	6-311G**	238 (18.5%)	6-311G**	251 (24.9%)
6-31+G(2df,p)	267 (33.3%)	6-31+G(2df,p)	244 (21.7%)	6-31+G(2df,p)	273 (36.3%)	6-31+G(2df,p)	234 (16.8%)	6-31+G(2df,p)	247 (23.1%)
revTPSS	E_0 (APD)	M06-L	E_0 (APD)	M06	E_0 (APD)	M06-2X	E_0 (APD)	ωB97x-D	E_0 (APD)
6-31G*	225 (12.3%)	6-31G*	226 (12.9%)	6-31G*	239 (19.3%)	6-31G*	299 (48.8%)	6-31G*	269 (33.9%)
6-311G**	234 (16.5%)	6-311G**	234 (16.4%)	6-311G**	244 (21.9%)	6-311G**	303 (51.0%)	6-311G**	275 (36.9%)
6-31+G(2df,p)	231 (15.1%)	6-31+G(2df,p)	235 (17.1%)	6-31+G(2df,p)	245 (22.1%)	6-31+G(2df,p)	298 (48.5%)	6-31+G(2df,p)	272 (35.6%)
CBS-QB3					196				
G3(MP2)-RAD					181				
G4(MP2)-6X					201				

Table 2. Energy Barrier (E_0) in kJ/mol for [2 + 2] Cycloaddition Reaction of Methyl Acrylate and Absolute Percent Deviation (APD) Relative to G4(MP2)-6X for Various Density Functionals and Basis Sets

| B3LYP	E_0 (APD)	PBE0	E_0 (APD)	BMK	E_0 (APD)	TPSS	E_0 (APD)	TPSSh	E_0 (APD)
6-31G*	187 (19.7%)	6-31G*	164 (4.8%)	6-31G*	196 (25.9%)	6-31G*	148 (5.3%)	6-31G*	162 (3.9%)
6-311G**	200 (28.1%)	6-311G**	173 (11.1%)	6-311G**	208 (33.2%)	6-311G**	159 (1.8%)	6-311G**	173 (10.7%)
6-31+G(2df,p)	203 (30.1%)	6-31+G(2df,p)	176 (12.8%)	6-31+G(2df,p)	209 (34.1%)	6-31+G(2df,p)	162 (3.5%)	6-31+G(2df,p)	175 (12.3%)
revTPSS	E_0 (APD)	M06-L	E_0 (APD)	M06	E_0 (APD)	M06-2X	E_0 (APD)	ωB97x-D	E_0 (APD)
6-31G*	140 (10.3%)	6-31G*	143 (8.3%)	6-31G*	165 (5.9%)	6-31G*	202 (29.4%)	6-31G*	195 (24.7%)
6-311G**	151 (2.9%)	6-311G**	153 (1.7%)	6-311G**	174 (11.4%)	6-311G**	210 (34.8%)	6-311G**	204 (30.7%)
6-31+G(2df,p)	155 (0.9%)	6-31+G(2df,p)	158 (1.6%)	6-31+G(2df,p)	180 (15.6%)	6-31+G(2df,p)	214 (37.1%)	6-31+G(2df,p)	207 (32.7%)
CBS-QB3					154				
G3(MP2)-RAD					146				
G4(MP2)-6X					156				

Table 3. Energy Barrier (E_0) in kJ/mol for [2 + 4] Cycloaddition Reaction of Methyl Acrylates and Absolute Percent Deviation (APD) Relative to G4(MP2)-6X for Various Density Functionals and Basis Sets

B3LYP	E_0 (APD)	PBE0	E_0 (APD)	BMK	E_0 (APD)	TPSS	E_0 (APD)	TPSSh	E_0 (APD)
6-31G*	128 (17.3%)	6-31G*	103 (5.5%)	6-31G*	126 (15.6%)	6-31G*	98 (9.6%)	6-31G*	108 (1.1%)
6-311G**	133 (22.2%)	6-311G**	102 (6.4%)	6-311G**	129 (18.1%)	6-311G**	95 (12.6%)	6-311G**	104 (4.3%)
6-31+G(2df,p)	139 (28.0%)	6-31+G(2df,p)	108 (1.1%)	6-31+G(2df,p)	134 (23.1%)	6-31+G(2df,p)	101 (7.5%)	6-31+G(2df,p)	110 (0.7%)
revTPSS	E_0 (APD)	M06-L	E_0 (APD)	M06	E_0 (APD)	M06-2X	E_0 (APD)	ωB97x-D	E_0 (APD)
6-31G*	89 (18.2%)	6-31G*	99 (9.4%)	6-31G*	114 (4.7%)	6-31G*	121 (11.3%)	6-31G*	123 (12.6%)
6-311G**	83 (24.1%)	6-311G**	88 (19.4%)	6-311G**	100 (8.5%)	6-311G**	111 (2.3%)	6-311G**	115 (5.5%)
6-31+G(2df,p)	89 (18.3%)	6-31+G(2df,p)	95 (12.7%)	6-31+G(2df,p)	109 (0.0%)	6-31+G(2df,p)	119 (9.3%)	6-31+G(2df,p)	122 (11.9%)
CBS-QB3					110				
G3(MP2)-RAD					108				
G4(MP2)-6X					109				

that the electronic structure of the diradical transition state of [2 + 2] cycloaddition is significantly different from the concerted pericyclic transition state of [2 + 4] cycloaddition.[30,54] The [2 + 2] cycloaddition reactions of acrylates are responsible for self-initiation of the monomers. Based upon these, we select TPSS/6-31G*, TPSSh/6-31G*, and PBE0/6-31G* due to their superior performances and lower computation costs in studying the [2 + 2] cycloaddition reactions to carry out further calculations described in the next sections.

3.2. Monomer Self-Initiation of MA. We identified the MECP in the monomer self-initiation of MA using PBE0/6-31G*, TPSS/6-31G*, and TPSSh/6-31G*.[55] T1 diagnostic reveals that the MECP optimized with PBE0/6-31G* has $T_1 = 0.017$, and the transition state for the spin-allowed [2 + 2] cycloaddition reaction has $T_1 = 0.021$, both showing large multireference character. The spin−orbit coupling matrix element H_{12} at the crossing point is computed using CASSCF

wavefunctions with eight active electrons in eight active orbitals. We designed the active space by selecting four π orbitals from each acrylate molecule (π and π^* orbitals from the C=C bond, and π and π^* orbitals from the C=O bond). This construction allows an appropriate description of diradical intermediate (breakage of the C=C π bond and formation of the C−C σ bond) and also includes possible effects from nearby C=O groups. The optimized active space is shown in Figure 3a. The H_{12} estimated with SO−CI at the MECP optimized by PBE0/6-31G* is 0.94 cm^{-1}, which is close to the value (1.63 cm^{-1}) obtained using SO-MCQDPT2. Both methods suggest a weak spin−orbit coupling at the crossing point. The partition functions of the reactants and MECPs are constructed as products of rigid-rotor and harmonic-oscillator terms. It should be noted that only the vibrational frequencies within the seam of crossing ($3N − 7$ vibrational modes) are used for estimating the vibrational partition function of MECP. Table 4 gives the values of H_{12}, μ, F, ΔF, E_c, crossing coefficient
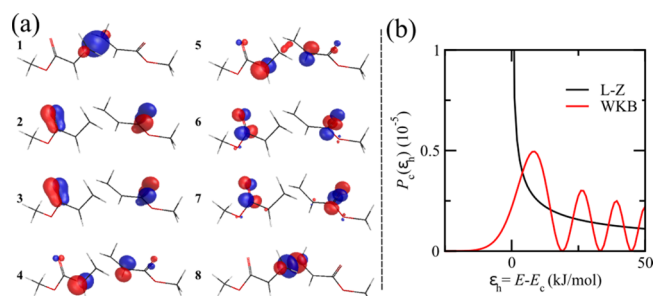
Figure 3. (a) Optimized CASSCF(8,8) active space at the MECP. (b) Intersystem crossing probability as a function of energy relative to the MECP in monomer self-initiation reaction of methyl acrylate given by the Landau−Zener (L−Z) formula and by the WKB theory.

$\Gamma(T)$, and rate constants k (both adiabatic k^A assuming unit crossing probability and nonadiabatic k^{NA}) at various temperatures. The energies of the MECP relative to reactants predicted with the three functionals are very close to each other (within 5 kJ/mol). This is consistent with our benchmark study in which PBE0, TPSS, and TPSSh give similar energy barrier values for the [2 + 2] cycloaddition reaction of MA. Figure 3b shows the energy-dependence of the crossing probability given by the Landau−Zener formula and the WKB theory. The L−Z curve goes to infinity at the crossing point ($E = E_c$) and drops to zero for energies below E_c, while $P_c^{WKB}(\varepsilon_h)$ has nonzero value below E_c and oscillates above E_c due to the interference between single-passage and double-passage paths. From Table 4, we find that the crossing coefficient does not change significantly above room temperature. Our results show that low crossing probability results in a small crossing coefficient $\sim 10^{-5}$, causing the nonadiabatic rate constant 5 orders of magnitude lower than the adiabatic rate coefficient assuming unit crossing probability. These results highlight that the intersystem crossing is very likely a rate-limiting step in the self-initiation reaction.

3.3. Electronic Structure of the Crossing Seam. The electronic structure of the crossing seam is explored by constructing the singlet and triplet potential energy surfaces (PESs) around the MECP. Single-point energy calculations are carried out for various combinations of bond length $r(C1−C3)$ and dihedral angle $\Phi(C4−C3−C2−C1)$ with PBE0/6-31G* (atom labels are shown in Figure 4). The 2D PESs are presented in Figure 4a,b, and the crossing seam is determined in Figure 4c and plotted in each map. The results show that the minimum of the triplet PES is located along the path of spin-

allowed [2 + 2] cycloaddition reaction and before the formation of the singlet transition state (with Φ approaching zero for ring closure). This electronic feature provides the tendency of intersystem crossing from singlet state to triplet state. Second, the crossing seam spans a variety of structures with similar singlet-state energies (within 10 kJ/mol) for $-180°$ $< \Phi < -60°$ as $r \approx 1.7$ Å, suggesting a flat energy profile within the crossing seam for a relatively large portion of configuration space. The flat energy surface most likely promotes the crossing events due to the availability of more energetically accessible configurations at a given temperature. In addition, within the crossing seam, the MECP is found to be closest to the minimum of the triplet PES without any barrier in between, which suggests that the relaxation after the intersystem crossing is spontaneous. We further calculate the spin−orbit coupling matrix elements for all the structures with individually optimized CASSCF wave functions. A 2D map of the corresponding H_{12} values is shown in Figure 4d; the H_{12} values are small and insensitive to the structural change.

3.4. Monomer Self-Initiation Reactions of EA, nBA, and MMA. The spin-forbidden transitions in polymerization of ethyl acrylate (EA), n-butyl acrylate (nBA), and methyl methacrylate (MMA) are studied using PBE0/6-31G*. Results given in Table 5 indicate that the overall nonadiabatic rate coefficients are on the same order for MA, EA, and nBA. This indicates that the size of the end-substituent alkyl group has little influence on the energy of the MECP and the crossing probability. The calculated k^{NA} at 413 K (1.04×10^{-14} M^{-1} s^{-1}) for the monomer self-initiation reaction of nBA agrees reasonably well with the value obtained from a mechanistic model (1.0×10^{-13} M^{-1} s^{-1}).[56] In the case of methyl methacrylate, the hopping probability is similar to that of acrylates, but the barrier between reactants and MECP is lower than that of acrylates, which is likely due to the stabilization effect of the methyl group attached to the tertiary carbon. The rate coefficients of MMA self-initiation reactions are 3−4 orders higher than those of acrylates.

3.5. Crossing Control. The higher rate constant for MMA suggests a potential route to achieve faster self-initiation: lowering the energy of the MECP by stabilizing the diradical with favorable functional groups. It is also possible to tune the rate constant via "crossing control", that is, promoting intersystem crossing by heavy-atom substitution. To this end, the four types of halogen-substituted methyl acrylates shown in Figure 5 are studied. The MECPs for F-, Cl-, and Br-substituted methyl acrylates are optimized with PBE0/6-31G*. For I-substituted methyl acrylate, we use Huzinaga's model core

Table 4. Spin-Orbit Coupling Matrix Element H_{12} in cm^{-1}, μ in Atomic Mass Unit, F and ΔF in Hartree/Bohr, and Crossing Energy E_c in kJ/mol for Methyl Acrylate Calculated with PBE0/6-31G*, TPSS/6-31G*, and TPSSh/6-31G*[a]

	PBE0/6-31G*			TPSSh/6-31G*			TPSS/6-31G*		
H_{12}	0.94			1.33			1.26		
μ	11.8671			11.8574			11.8613		
F	0.07526			0.05307			0.06465		
ΔF	0.15721			0.10648			0.13059		
E_c	127.5			130.5			124.6		
T	298	393	413	298	393	413	298	393	413
$\Gamma(T)$	9.73×10^{-5}	2.20×10^{-5}	1.91×10^{-5}	1.34×10^{-4}	4.44×10^{-5}	3.99×10^{-5}	8.20×10^{-5}	4.09×10^{-5}	3.80×10^{-5}
$k^A(T)$	2.71×10^{-16}	8.22×10^{-11}	5.75×10^{-10}	5.03×10^{-17}	2.06×10^{-11}	1.50×10^{-10}	8.17×10^{-16}	1.84×10^{-10}	1.23×10^{-9}
$k^{NA}(T)$	2.64×10^{-20}	1.80×10^{-15}	1.10×10^{-14}	6.73×10^{-21}	9.14×10^{-16}	5.99×10^{-15}	6.70×10^{-20}	7.52×10^{-15}	4.68×10^{-14}

[a]The crossing coefficient $\Gamma(T)$, and adiabatic rate constant $k^A(T)$ without crossing correction and non-adiabadic rate constant $k^{NA}(T)$ in M^{-1} s^{-1} at various temperatures (T in K) are evaluated from the WKB theory.
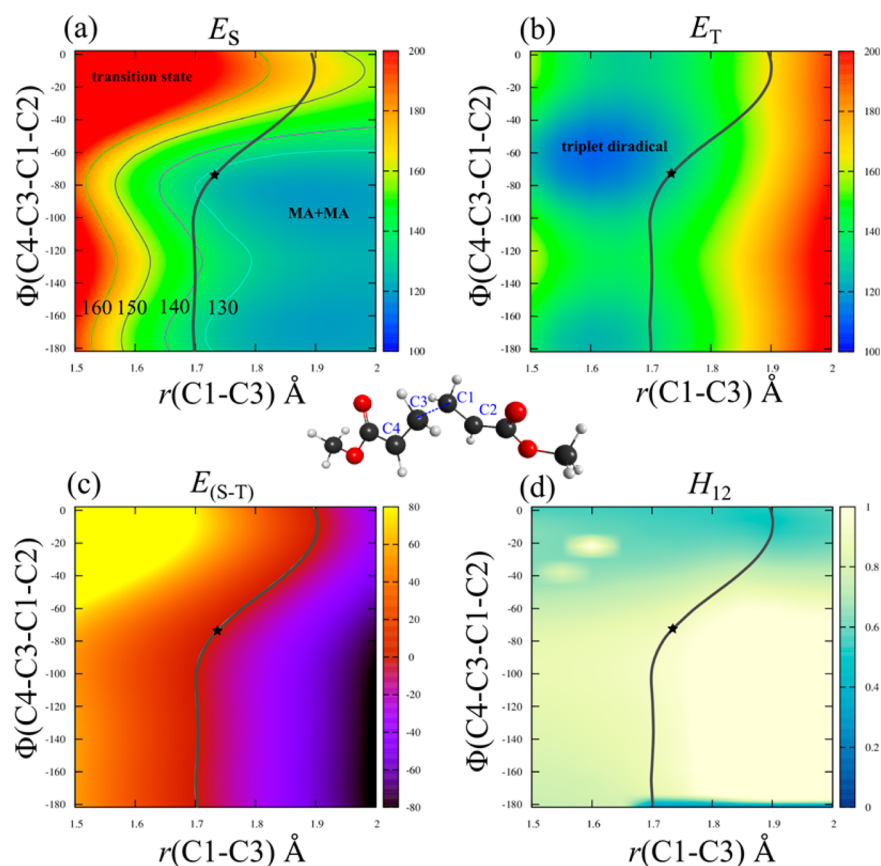
Figure 4. (a) Singlet potential energy surface, (b) triplet potential energy surface, (c) singlet−triplet energy difference in kJ/mol, and (d) spin−orbit coupling matrix element in cm^{-1}. Each is a 2D map as a function of bond length r(C1−C3) and dihedral angle Φ(C4−C3−C2−C1). The black line in each map represents the crossing seam ($E_{S\text{-}T}$ = 0.0 kJ/mol). The star symbol represents the MECP.

Table 5. Spin-Orbit Coupling Matrix Element H_{12} in cm^{-1}, μ in Atomic Mass Unit, F and ΔF in Hartree/Bohr, and Crossing Energy E_c in kJ/mol for EA, n-BA, and MMA Calculated with PBE0/6-31G^{*a}

	EA			nBA			MMA		
H_{12}	0.78			0.83			1.35		
μ	11.8689			11.8667			12.1047		
F	0.07569			0.07589			0.05205		
ΔF	0.15821			0.15878			0.10749		
E_c	127.4			128.4			98.7		
T	298	393	413	298	393	413	298	393	413
$\Gamma(T)$	6.81×10^{-5}	1.51×10^{-5}	1.31×10^{-5}	7.75×10^{-5}	1.70×10^{-5}	1.48×10^{-5}	8.33×10^{-5}	4.52×10^{-5}	4.23×10^{-5}
$k^A(T)$	8.37×10^{-17}	2.79×10^{-11}	1.97×10^{-10}	2.98×10^{-16}	9.95×10^{-11}	7.03×10^{-10}	5.31×10^{-12}	9.19×10^{-8}	4.13×10^{-7}
$k^{NA}(T)$	5.70×10^{-21}	4.21×10^{-16}	2.58×10^{-15}	2.31×10^{-20}	1.69×10^{-15}	1.04×10^{-14}	4.42×10^{-16}	4.16×10^{-12}	1.75×10^{-11}

^{a}The crossing coefficient $\Gamma(T)$, and adiabatic rate constant $k^A(T)$ without crossing correction and non-adiabadic rate constant $k^{NA}(T)$ in M^{-1} s^{-1} at various temperatures (T in K) are evaluated from the WKB theory.
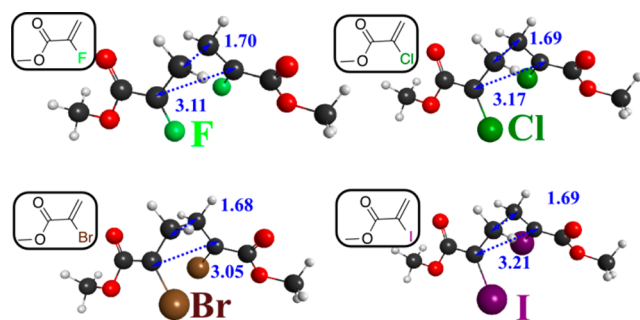

Figure 5. MECPs for four types of halogen-substituted methyl acrylates.

potential (MCP)[57,58] and the matched MCP-dzp basis set[59] to identify the MECP. Figure 5 presents the structures of the optimized MECPs. Table 6 gives the values of H_{12} and crossing energies. We also evaluate the effect of basis set on the magnitude of H_{12} for Br-substituted MA. The value of H_{12}

Table 6. Spin-Orbit Coupling Matrix Element H_{12} in cm^{-1} and Crossing Energy E_c in kJ/mol for Halogen-Substituted Methyl Acrylates

	F	Cl	Br	I
H_{12}	0.61	1.69	7.86	10.7
E_c	100	82.5	91.6	92.5

obtained with 6-31G*, MCP-dzp, and MCP-tzp are 7.85, 5.94, and 5.71 cm^{-1}, respectively. The halogen-substitution appears to stabilize the MECP, which is likely due to the resonance donation of electron density from the halogen lone pair to the attached carbon. This is confirmed by Natural Bond Orbital (NBO) analysis[60] that the occupancy of NBO at the radical center (shown in Figure 6) increases from 0.97577 in MA to
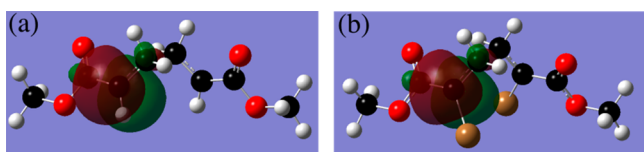
Figure 6. NBO at radical center for the MECP of (a) methyl acrylate and (b) Br-substitute methyl acrylate.

1.09487 (increased by 12.2%) in Br-substituted MA. Furthermore, heavy halogen atoms, such as Br and I, significantly increase the magnitude of spin−orbit coupling, which is expected to induce higher probability of crossing from the singlet state to the triplet state. The nonadiabatic rate constant for the self-initiation reaction of Br-substituted methyl acrylates is found to be 5.66×10^{-14} M^{-1} s^{-1} at 298 K with a crossing probability of 2.0×10^{-3}, which are significantly higher than for MA ($k^{NA} = 2.64 \times 10^{-20}$ M^{-1} s^{-1} with $\Gamma = 9.7 \times 10^{-5}$). This agrees with previous experimental observations that halogen-containing acrylate monomers polymerize at a much higher rate.[61]

4. CONCLUSIONS

The benchmark study of [2 + 2] cycloaddition reaction of methyl acrylate presented in this paper indicated that special attention is required for reactions involving diradicals in order to predict energy barriers reliably. PBE0, TPSSh, and in particular TPSS with a 6-31G* basis set are computationally efficient levels of theory for exploring monomer self-initiation reactions of acrylates. We applied nonadiabatic transition-state theory based on the WKB theory of crossing probability to describe the kinetics of the monomer self-initiation reactions. We found that intersystem crossing of a singlet diradical to a triplet diradical is a rate-limiting step in self-initiation. Methyl methacrylate has a higher rate constant than acrylates studied in this work, which is due to the lower energy barrier between MMA and the crossing point. Crossing control via heavy-atom substitution was demonstrated and is likely to provide a new route of applying spin-chemistry in free-radical polymerization.

ASSOCIATED CONTENT

S Supporting Information

Derivations of the crossing coefficient in the nonadiabatic transition state theory. Structures and vibrational frequencies at stationary points, transition states, and minimum energy crossing points. This material is available free of charge via the Internet at http://pubs.acs.org.

AUTHOR INFORMATION

Corresponding Author

*E-mail: rappe@sas.upenn.edu.

Notes

The authors declare no competing financial interest.

REFERENCES

(1) Eyring, H. The Activated Complex in Chemical Reactions. *J. Chem. Phys.* **1935**, *3*, 107−15.

(2) Marian, C. M. Spin-Orbit Coupling and Intersystem Crossing in Molecules. *WIREs Comput. Mol. Sci.* **2012**, *2*, 187−203.

(3) Harvey, J. N. Spin-Forbidden Reactions: Computational Insight into Mechanisms and Kinetics. *WIREs Comput. Mol. Sci.* **2014**, *4*, 1−14.

(4) Harvey, J. N. Understanding the Kinetics of Spin-Forbidden Chemical Reactions. *Phys. Chem. Chem. Phys.* **2007**, *9*, 331−43.

(5) Khudyakov, I. V.; Serebrennikov, Y. A.; Turro, N. J. Spin-Orbit Coupling in Free-Radical Reactions: On the Way to Heavy Elements. *Chem. Rev. (Washington, DC, U. S.)* **1993**, *93*, 537−70.

(6) Dirac, P. A. M. The Quantum Theory of the Electron. *Proc. R. Soc. London, Ser. A* **1928**, *117*, 610−24.

(7) Lehnert, N.; Ho, R. Y. N.; Que, L.; Solomon, E. I. Spectroscopic Properties and Electronic Structure of Low-Spin Fe (III)-Alkylperoxo Complexes: Homolytic Cleavage of the O-O Bond. *J. Am. Chem. Soc.* **2001**, *123*, 8271−90.

(8) Harvey, J. N.; Aschi, M. Modelling Spin-Forbidden Reactions: Recombination of Carbon Monoxide with Iron Tetracarbonyl. *Faraday Discuss.* **2003**, *124*, 129−43.

(9) Srinivasan, S.; Kalfas, G.; Petkovska, V. I.; Bruni, C.; Grady, M. C.; Soroush, M. Experimental Study of the Spontaneous Thermal Homopolymerization of Methyl and *n*-Butyl Acrylate. *J. Appl. Polym. Sci.* **2010**, *118*, 1898−909.

(10) Srinivasan, S.; Lee, M. W.; Grady, M. C.; Soroush, M.; Rappe, A. M. Computational Study of the Self-Initiation Mechanism in Thermal Polymerization of Methyl Acrylate. *J. Phys. Chem. A* **2009**, *113*, 10787−94.

(11) Srinivasan, S.; Lee, M. W.; Grady, M. C.; Soroush, M.; Rappe, A. M. Self-Initiation Mechanism in Spontaneous Thermal Polymerization of Ethyl and *n*-Butyl Acrylate: A Theoretical Study. *J. Phys. Chem. A* **2010**, *114*, 7975−83.

(12) Srinivasan, S.; Lee, M. W.; Grady, M. C.; Soroush, M.; Rappe, A. M. Computational Evidence for Self-Initiation in Spontaneous High-Temperature Polymerization of Methyl Methacrylate. *J. Phys. Chem. A* **2011**, *115*, 1125−32.

(13) Quan, C. L.; Soroush, M.; Grady, M. C.; Hansen, J. E.; Simonsick, W. J. High-Temperature Homopolymerization of Ethyl Acrylate and *n*-Butyl Acrylate: Polymer Characterization. *Macromolecules* **2005**, *38*, 7619−28.

(14) Doering, W. v. E.; Ekmanis, J. L.; Belfield, K. D.; Klärner, F. G.; Krawczyk, B. Thermal Reactions of *anti*- and *syn*-Dispiro[5.0.5.2]-tetradeca-1,8-dienes: Stereomutation and Fragmentation to 3-Methyl-enecyclohexenes. Entropy-Dictated Product Ratios from Diradical Intermediates? *J. Am. Chem. Soc.* **2001**, *123*, 5532−41.

(15) Klärner, F.-G.; Wurche, F.; Doering, W. v. E.; Yang, J. Pressure Independence of Stereomutation and Fragmentation in the Bis-spirocyclobutanes, *anti*- and *syn*-2,9-Dicyanodispiro[5.0.5.2]tetradeca-1,8-dienes. *J. Am. Chem. Soc.* **2005**, *127*, 18107−13.

9316

dx.doi.org/10.1021/jp503794j | *J. Phys. Chem. A* 2014, 118, 9310−9318

(16) Harvey, J. N.; Aschi, M. Spin-Forbidden Dehydrogenation of Methoxy Cation: A Statistical View. *Phys. Chem. Chem. Phys.* **1999**, *1*, 5555−63.

(17) Jasper, A. W.; Dawes, R. Non-Born-Oppenheimer Molecular Dynamics of the Spin-Forbidden Reaction $O(^3P)+CO(X^1\Sigma^+)\rightarrow CO_2(X^1\Sigma_g^+)$. *J. Chem. Phys.* **2013**, *139*, 154313.

(18) Forst, W. *Unimolecular Reactions: A Concise Introduction*; Cambridge University Press, 2003.

(19) Rubbmark, J. R.; Kash, M. M.; Littman, M. G.; Kleppner, D. Dynamical Effects at Avoided Level-Crossings: A Study of the Landau-Zener Effect Using Rydberg Atoms. *Phys. Rev. A* **1981**, *23*, 3107−17.

(20) Zener, C. Dissociation of Excited Diatomic Molecules by External Perturbations. *Proc. R. Soc. London, Ser. A* **1933**, *140*, 660−68.

(21) Wittig, C. The Landau-Zener Formula. *J. Phys. Chem. B* **2005**, *109*, 8428−30.

(22) Nikitin, E. E.; Kearsley, M. J. *Theory of Elementary Atomic and Molecular Processes in Gases*; Clarendon Press: Oxford, 1974.

(23) Delos, J. B. Reactions of N_2 with O. *J. Chem. Phys.* **1973**, *59*, 2365−69.

(24) Fedorov, D. G.; Koseki, S.; Schmidt, M. W.; Gordon, M. S. Spin-Orbit Coupling in Molecules: Chemistry Beyond the Adiabatic Approximation. *Int. Rev. Phys. Chem.* **2003**, *22*, 551−92.

(25) Koseki, S.; Fedorov, D. G.; Schmidt, M. W.; Gordon, M. S. Spin-Orbit Splittings in the Third-Row Transition Elements: Comparison of Effective Nuclear Charge and Full Breit-Pauli Calculations. *J. Phys. Chem. A* **2001**, *105*, 8262−68.

(26) Furlani, T. R.; King, H. F. Theory of Spin-Orbit Coupling. Application to Singlet-Triplet Interaction in the Trimethylene Biradical. *J. Chem. Phys.* **1985**, *82*, 5577−83.

(27) King, H. F.; Furlani, T. R. Computation of One and Two Electron Spin-Orbit Integrals. *J. Comput. Chem.* **1988**, *9*, 771−78.

(28) Noble, B. B.; Coote, M. L. First Principles Modelling of Free-Radical Polymerisation Kinetics. *Int. Rev. Phys. Chem.* **2013**, *32*, 467−513.

(29) Montgomery, J. A., Jr; Frisch, M. J.; Ochterski, J. W.; Petersson, G. A. A Complete Basis Set Model Chemistry. VI. Use of Density Functional Geometries and Frequencies. *J. Chem. Phys.* **1999**, *110*, 2822−27.

(30) Ess, D. H.; Houk, K. N. Activation Energies of Pericyclic Reactions: Performance of DFT, MP2, and CBS-QB3Methods for the Prediction of Activation Barriers and Reaction Energetics of 1,3-Dipolar Cycloadditions, and Revised Activation Enthalpies for a Standard Set of Hydrocarbon Pericyclic Reactions. *J. Phys. Chem. A* **2005**, *109*, 9542−53.

(31) Henry, D. J.; Sullivan, M. B.; Radom, L. G3-RAD and G3X-RAD: Modified Gaussian-3 (G3) and Gaussian-3X (G3X) Procedures for Radical Thermochemistry. *J. Chem. Phys.* **2003**, *118*, 4849−60.

(32) Chan, B.; Deng, J.; Radom, L. G4(MP2)-6X: A Cost-Effective Improvement to G4(MP2). *J. Chem. Theory Comput.* **2011**, *7*, 112−20.

(33) Chan, B.; Radom, L. BDE261: A Comprehensive Set of High-Level Theoretical Bond Dissociation Enthalpies. *J. Phys. Chem. A* **2012**, *116*, 4975−86.

(34) Liu, S.; Srinivasan, S.; Grady, M. C.; Soroush, M.; Rappe, A. M. Backbiting and β-Scission Reactions in Free-Radical Polymerization of Methyl Acrylate. *Int. J. Quantum Chem.* **2014**, *114*, 345−60.

(35) Frisch, M. J.; Trucks, G. W.; Schlegel, H. B.; Scuseria, G. E.; Robb, M. A.; Cheeseman, J. R.; Scalmani, G.; Barone, V.; Mennucci, B.; Petersson, G. A.; Nakatsuji, H.; Caricato, M.; Li, X.; Hratchian, H. P.; Izmaylov, A. F.; Bloino, J.; Zheng, G.; Sonnenberg, J. L.; Hada, M.; Ehara, M.; Toyota, K.; Fukuda, R.; Hasegawa, J.; Ishida, M.; Nakajima, T.; Honda, Y.; Kitao, O.; Nakai, H.; Vreven, T.; Montgomery, J. A., Jr.; Peralta, J. E.; Ogliaro, F.; Bearpark, M.; Heyd, J. J.; Brothers, E.; Kudin, K. N.; Staroverov, V. N.; Kobayashi, R.; Normand, J.; Raghavachari, K.; Rendell, A.; Burant, J. C.; Iyengar, S. S.; Tomasi, J.; Cossi, M.; Rega, N.; Millam, M. J.; Klene, M.; Knox, J. E.; Cross, J. B.; Bakken, V.; Adamo, C.; Jaramillo, J.; Gomperts, R.; Stratmann, R. E.; Yazyev, O.; Austin, A. J.; Cammi, R.; Pomelli, C.; Ochterski, J. W.; Martin, R. L.; Morokuma, K.; Zakrzewski, V. G.; Voth, G. A.; Salvador, P.; Dannenberg, J. J.; Dapprich, S.; Daniels, A. D.; Farkas, Ö.;

Foresman, J. B.; Ortiz, J. V.; Cioslowski, J.; Fox, D. J. Gaussian 09; Gaussian. Inc., Wallingford, CT, 2009.

(36) Becke, A. D. Density-Functional Thermochemistry. III. The Role of Exact Exchange. *J. Chem. Phys.* **1993**, *98*, 5648−52.

(37) Stephens, P. J.; Devlin, F. J.; Chabalowski, C. F.; Frisch, M. J. *Ab Initio* Calculation of Vibrational Absorption and Circular Dichroism Spectra Using Density Functional Force Fields. *J. Phys. Chem.* **1994**, *98*, 11623−27.

(38) Hertwig, R. H.; Koch, W. On the Parameterization of the Local Correlation Functional. What Is Becke-3-LYP? *Chem. Phys. Lett.* **1997**, *268*, 345−51.

(39) Adamo, C.; Barone, V. Toward Reliable Density Functional Methods without Adjustable Parameters: The Pbe0 Model. *J. Chem. Phys.* **1999**, *110*, 6158−70.

(40) Boese, A. D.; Martin, J. M. Development of Density Functionals for Thermochemical Kinetics. *J. Chem. Phys.* **2004**, *121*, 3405−16.

(41) Tao, J.; Perdew, J. P.; Staroverov, V. N.; Scuseria, G. E. Climbing the Density Functional Ladder: Nonempirical Meta-Generalized Gradient Approximation Designed for Molecules and Solids. *Phys. Rev. Lett.* **2003**, *91*, 146401 (1−4)..

(42) Staroverov, V. N.; Scuseria, G. E.; Tao, J.; Perdew, J. P. Comparative Assessment of a New Nonempirical Density Functional: Molecules and Hydrogen-Bonded Complexes. *J. Chem. Phys.* **2003**, *119*, 12129−37.

(43) Perdew, J. P.; Ruzsinszky, A.; Csonka, G. I.; Constantin, L. A.; Sun, J. Workhorse Semilocal Density Functional for Condensed Matter Physics and Quantum Chemistry. *Phys. Rev. Lett.* **2009**, *103*, 026403.

(44) Zhao, Y.; Truhlar, D. G. A New Local Density Functional for Main-Group Thermochemistry, Transition Metal Bonding, Thermochemical Kinetics, and Noncovalent Interactions. *J. Chem. Phys.* **2006**, *125*, 194101.

(45) Zhao, Y.; Truhlar, D. G. The M06 Suite of Density Functionals for Main Group Thermochemistry, Thermochemical Kinetics, Noncovalent Interactions, Excited States, and Transition Elements: Two New Functionals and Systematic Testing of Four M06-Class Functionals and 12 Other Functionals. *Theor. Chem. Acc.* **2008**, *120*, 215−41.

(46) Chai, J. D.; Head-Gordon, M. Long-Range Corrected Hybrid Density Functionals with Damped Atom-Atom Dispersion Corrections. *Phys. Chem. Chem. Phys.* **2008**, *10*, 6615−20.

(47) Schmidt, M. W.; Baldridge, K. K.; Boatz, J. A.; Elbert, S. T.; Gordon, M. S.; Jensen, J. H.; Koseki, S.; Matsunaga, N.; Nguyen, K. A.; Su, S.; Windus, T. L.; Dupuis, M.; Montgomery, J. A., Jr. General Atomic and Molecular Electronic-Structure System. *J. Comput. Chem.* **1993**, *14*, 1347−63.

(48) Wong, M. W.; Radom, L. Radical Addition to Alkenes: an Assessment of Theoretical Procedures. *J. Phys. Chem.* **1995**, *99*, 8582−88.

(49) Wong, M. W.; Radom, L. Radical Addition to Alkenes: Further Assessment of Theoretical Procedures. *J. Phys. Chem. A* **1998**, *102*, 2237−45.

(50) Fedorov, D. G.; Finley, J. P. Spin-Orbit Multireference Multistate Perturbation Theory. *Phys. Rev. A* **2001**, *64*, 042502.

(51) Gannon, K. L.; Blitz, M. A.; Liang, C. H.; Pilling, M. J.; Seakins, P. W.; Glowacki, D. R.; Harvey, J. N. An Experimental and Theoretical Investigation of the Competition between Chemical Reaction and Relaxation for the Reactions of $^1CH_2$ with Acetylene and Ethene: Implications for the Chemistry of the Giant Planets. *Faraday Discuss.* **2010**, *147*, 173−88.

(52) Harvey, J. N.; Aschi, M.; Schwarz, H.; Koch, W. The Singlet and Triplet States of Phenyl Cation. A Hybrid Approach for Locating Minimum Energy Crossing Points between Non-Interacting Potential Energy Surfaces. *Theor. Chem. Acc.* **1998**, *99*, 95−99.

(53) Quick, L. M.; Knecht, D. A.; Back, M. H. Kinetics of the Formation of Cyclobutane from Ethylene. *Int. J. Chem. Kinet.* **1972**, *4*, 61−68.

(54) Liu, S.; Srinivasan, S.; Grady, M. C.; Soroush, M.; Rappe, A. M. Computational Study of Cyclohexanone-Monomer Co-Initiation

Mechanism in Thermal Homo-Polymerization of Methyl Acrylate and Methyl Methacrylate. *J. Phys. Chem. A* **2012**, *116*, 5337−48.

(55) Lee, T. J.; Taylor, P. R. A Diagnostic for Determining the Quality of Single-Reference Electron Correlation Methods. *Int. J. Quantum Chem.* **1989**, *36*, 199−207.

(56) Moghadam, N. Computational Study of Chain Transfer Reactions in Self-Initiated High-Temperature Polymerization of Alkyl Acrylates. Ph.D. Thesis, Drexel University, Philadelphia, PA, 2014.

(57) Miyoshi, E.; Sakai, Y.; Tanaka, K.; Masamura, M. Relativistic *dsp*-Model Core Potentials for Main Group Elements in the Fourth, Fifth and Sixth Row and Their Applications. *J. Mol. Struct. THEOCHEM* **1998**, *451*, 73−79.

(58) Sekiya, M.; Noro, T.; Osanai, Y.; Koga, T. Contracted Polarization Functions for the Atoms Ca, Ga-Kr, Sr, and In-Xe. *Theor. Chem. Acc.* **2001**, *106*, 297−300.

(59) Miyoshi, E.; Mori, H.; Hirayama, R.; Osanai, Y.; Noro, T.; Honda, H.; Klobukowski, M. Compact and Efficient Basis Sets of *s*- and *p*-Block Elements for Model Core Potential Method. *J. Chem. Phys.* **2005**, *122*, 074104.

(60) Foster, J. P.; Weinhold, F. Natural Hybrid Orbitals. *J. Am. Chem. Soc.* **1980**, *102*, 7211−18.

(61) Lingnau, J.; Meyerhoff, G. Spontaneous Polymerization of Methyl Methacrylate. 8. Polymerization Kinetics of Acrylates Containing Chlorine Atoms. *Macromolecules* **1984**, *17*, 941−45.